A Well-balanced Finite Volume Scheme for Shallow Water Equations with Porosity Application to Modelling of Open-Channel Flow through Rigid and Emergent Vegetation

Minh H. Le, Virgile Dubos, Marina Oukacine, Nicole Goutal

A Well-balanced Finite Volume Scheme for Shallow Water Equations with Porosity

Application to Modelling of Open-Channel Flow through Rigid and Emergent Vegetation

Minh H. Le[1,*], *Virgile* Dubos[3,**], *Marina* Oukacine[1,***], and *Nicole* Goutal[1,2,****]

[1]LHSV, 6 quai Watier, 78401 Chatou cedex, France
[2]EDF R&D, 6 quai Watier, 78401 Chatou cedex, France
[3]Sorbonne Université, Université Paris-Diderot SPC, CNRS, INRIA,
Laboratoire Jacques-Louis Lions, LJLL, ANGE, F-75005 Paris, France

Abstract. Strong interactions exist between flow dynamics and vegetation in open-channel. Depth-averaged shallow water equations can be used for such a study. However, explicit representation of vegetation can lead to very high resolution of the mesh since rigid vegetation is often modelled as vertical cylinders. Our work aims to study the ability of a single porosity-based shallow water model for these applications. More attention on flux and source terms discretizations are required in order to archive the well-balancing and shock capturing. We present a new Godunov-type finite volume scheme based on a simple-wave approximation and compare it with some other methods in the literature. A first application with experimental data was performed.

1 Introduction

Vegetation is known to play important role in dynamic of open-channel flow. Depending on the shape, density and spatial distribution of vegetation, water depth and flow direction might be significantly modified because the vegetation roughness is much larger than the roughness of river bed [1, 2]. Understanding the influence of vegetation on river flow, or more general in environmental fluid mechanics, have been primary interest for decades. Shallow Water (SW) model, obtaining by depth-integrating Navier-Stokes equations under shallowness hypothesis, can provide an accurate representation of physical processes of flow through vegetation. Nevertheless, such an *explicit* modelling is not suitable in the field, because it leads to very expensive computational cost; furthermore, the real geometry is generally not available or not accurate enough.

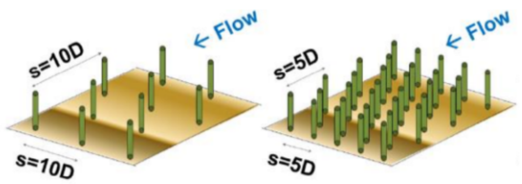

Figure 1. Flow through rigid vegetation with different densities. Credit: Y. Peltier.

*e-mail: minh-hoang.le@enpc.fr
**e-mail: dubos@ljll.math.upmc.fr
***e-mail: marina.oukacine@enpc.fr
****e-mail: nicole.goutal@edf.fr

It seems more appropriate to use *implicit* or *macroscopic* modelling for practical application. Traditional approaches consists in adding a drag force globally or locally into the momentum equation of SW model to enhance the determination of the local velocities. A more advanced macroscopic model, that we are interested here, is to introduce a porosity term into SW model. The porosity, ϕ, represents the fraction of the plan view area available to flow. For emergent and rigid vegetation, one can consider an isotropic and depth-independent porosity, see Fig. 1. This approach is called *single porosity* (SP) model [3] whose the mass and momentum conservation equations write

$$\begin{cases} \partial_t(\phi h) + \mathrm{div}\,(\phi h \mathbf{u}) = 0, \\ \partial_t(\phi h \mathbf{u}) + \mathrm{div}\,(\phi h \mathbf{u} \otimes \mathbf{u}) + \nabla\left(\dfrac{g}{2}\phi h^2\right) \\ \qquad\qquad = \dfrac{g}{2} h^2 \nabla\phi - g\phi h \nabla b - \tau_b - \tau_d, \end{cases} \tag{1}$$

where h represents the depth of water and $\mathbf{u}$ denotes the depth-averaged horizontal velocity with components u and v; g is the acceleration due to gravity, b is the bed elevation, τ_b stands for the friction stress and finally τ_d expresses the depth-integrated drag due to vegetation. These last two terms are estimated by empirical quadratic laws, writing

$$\tau_b = g\phi h \frac{n^2|\mathbf{u}|\mathbf{u}}{h^{4/3}}, \quad \tau_d = \frac{1}{2}\frac{aC_d h|\mathbf{u}|\mathbf{u}}{\phi} \tag{2}$$

in which n is Manning's coefficient and C_d is drag coefficient. The parameter $a = \frac{1-\phi}{\pi D/4}$ is often termed as *frontal area* of vegetation of effective diameter D. Since drag force acts upon the fluid which occupies only a fraction

ϕ of the total volume, the total drag is thus divided by ϕ. It is evident that when $\phi = 1$, we find again SW model.

Numerical scheme for SP model has been less studied than SW model. One can see from (1) that SP model presents an additional non-conservative source term due to spatial variation of porosity. Structure of the solution is thus mathematically more complex than SW model. In framework of finite volume method, a first scheme was proposed by Guinot and Soares-Frazão [4] in which the authors modified the numerical HLLC flux to account the porosity source term. This method is found to be efficient for shock capturing but it is inaccurate for steady solutions of the model. Next, several approaches of Roe-type have been proposed, one can cited [5–8]. All these methods reply on the Roe-averaged state of SW model and the source terms are next projected on the basis of eigenvectors of the linearized system. These approaches are known to have the same difficulties in preserving the positivity of water depth or when dealing with critical state (sonic point). We would like to mention here a third approach proposed by Finaud-Guyot et *al.* [9] which particularly holds our attention. Under assumption that all waves are rarefactions, the solution can entirely be determined using Riemann invariants. This solver, namely PorAS, is shown to be very accurate for regular solution, including the steady ones, but has difficulties for estimating shock waves.

We aim to study a robust scheme which inherits, on one hand, the good properties of HLLC solver, such as positivity preserving, shock capturing and easy to implement; on the other hand, the scheme captures accurately steady solutions as with PorAS method. Therefore, we have considered a suitable simple-wave approximation of solution on which exact Riemann invariants are imposed.

The paper is organized as follows: we first recall the two-dimension finite volume formalism whose numerical fluxes at each cell's interface are obtained by solving a projected one-dimension Riemann problem. Next, we detail and analyse the construction of the simple-solver. Two test cases for illustrating the attractive behaviours of the method are presented. Finally a real application with experimental data was performed.

2 Numerical scheme

We propose and analyse here a novel finite volume discretization for governing equations (1). It should be convenient to rewrite the system under vectorial form of a conservation law with source terms such as

$$\partial_t \mathbf{W} + \partial_x \mathbf{F} + \partial_y \mathbf{G} = \mathbf{S} - \mathbf{S}_\tau, \tag{3}$$

in which we have denoted the conservative variable $\mathbf{W} = (\phi h, \phi hu, \phi hv)^T$, the fluxes $\mathbf{F}(\mathbf{W}), \mathbf{G}(\mathbf{W})$, the non-conservative source term $\mathbf{S}(\mathbf{W}, b)$ due to bathymetry and porosity gradients, also the source term $\mathbf{S}_\tau(\mathbf{W})$ accounting the friction and additional drag. They write

$$\mathbf{F}(\mathbf{W}) = \begin{pmatrix} \phi hu \\ \phi hu^2 + \frac{g}{2}\phi h^2 \\ \phi huv \end{pmatrix}, \quad \mathbf{G}(\mathbf{W}) = \begin{pmatrix} \phi hv \\ \phi huv \\ \phi hv^2 + \frac{g}{2}\phi h^2 \end{pmatrix},$$
$$\mathbf{S}(\mathbf{W}, b) = \begin{pmatrix} 0 \\ \frac{g}{2}h^2\nabla\phi - g\phi h\nabla b \end{pmatrix}, \quad \mathbf{S}_\tau(\mathbf{W}) = \begin{pmatrix} 0 \\ \tau_b + \tau_d \end{pmatrix}.$$

2.1 Two-dimension finite volume formalism

Let Ω denote the computational domain discretized by a simplex mesh $\mathcal{T}_h$. For two adjacent cells C_j and C_k of the mesh, we denote Γ_{jk} their common edge and $\mathbf{n}_{jk} = (n_1, n_2)$ the outward unit normal vector to Γ_{jk}, from C_j to C_k.

Given an approximation $\{\phi, b\}_j$ of geometric data on the mesh and assuming that a piecewise constant approximation $\mathbf{W}_j^n$ at time $t^n = n\Delta t$ is known, that is by providing

$$\mathbf{W}_j^n = \frac{1}{|C_j|}\int_{C_j} \mathbf{W}(\mathbf{x}, t^n)\,\mathrm{d}\mathbf{x}$$

with $\mathbf{x} = (x, y)$ the space coordinates, Δt the time step, finite volume scheme consists in computing the updated solution $\mathbf{W}_j^{n+1}$ at next time level $t^{n+1} = t^n + \Delta t$.

Well-balanced scheme, i.e. that preserves at least the steady state at rest ($\mathbf{u} = 0,\ h + b = \text{const.}$), becomes nowadays a prerequisite criteria for modern numerical method. A classical way to design such a discretization for shallow water model is to solve system (3) in two following steps.

Convection. In order to balance the convective terms and the geometrical source terms, i.e. which contain gradient of ϕ and b, we solve first the following PDE system

$$\begin{cases} \partial_t \mathbf{W} + \partial_x \mathbf{F} + \partial_y \mathbf{G} = \mathbf{S}, \\ \mathbf{W}(\mathbf{x}, 0) = \mathbf{W}^n. \end{cases} \tag{4}$$

This results an intermediate solution denoted $\mathbf{W}_j^{n+1/2}$. Integrating (4) over a space-time control volume $C_j \times (t^n, t^{n+1})$ and applying the divergence theorem, the resulting numerical scheme can be written under the form

$$\mathbf{W}_j^{n+1/2} = \mathbf{W}_j^n - \frac{\Delta t}{|C_j|}\sum_{\Gamma_{jk}\subset\partial C_j} |\Gamma_{jk}|\mathcal{F}(\mathbf{W}_j^n, \mathbf{W}_k^n; b_j, b_k), \tag{5}$$

in which $\mathcal{F}(\mathbf{W}_j^n, \mathbf{W}_k^n; b_j, b_k)$ is an approximation of flux and source terms along the edge Γ_{jk} and in direction $\mathbf{n}_{jk}$. Therefore, constructing a two-dimension scheme consists in providing a numerical flux $\mathcal{F}$. Thanks to *rotational invariance* property, that is $n_1\mathbf{F}(\mathbf{W}) + n_2\mathbf{G}(\mathbf{W}) = R_{\mathbf{n}_{ij}}^{-1}\mathbf{F}(R_{\mathbf{n}_{ij}}\mathbf{W})$ with $R_{\mathbf{n}_{ij}}$ being the rotation matrix, the numerical flux can thus be derived from the one-dimension system. This later will be detailed in the next section.

Friction and drag. Once the state $\mathbf{W}_j^{n+1/2}$ is known, the next step is to account the friction and drag momentum source terms by solving

$$\begin{cases} \partial_t \mathbf{W} = -\mathbf{S}_\tau, \\ \mathbf{W}(\mathbf{x}, 0) = \mathbf{W}^{n+1/2}. \end{cases} \tag{6}$$

Similarity to the case of SW model, this ODE system can be discretized by a semi-implicit scheme which ensures the stability of the solution and is known to be very efficient for wet/dry transition [10]. Regarding empirical law (2), numerical discretization for system (6) writes

$$\begin{cases} h_j^{n+1} = h_j^{n+1/2}, \\ (\phi h\mathbf{u})_j^{n+1} = \dfrac{(\phi h\mathbf{u})_j^{n+1/2}}{1+\Delta t\left(\frac{n^2 g|\mathbf{u}_j^n|}{(h_j^{n+1})^{4/3}} + \frac{1}{2}\frac{aC_d|\mathbf{u}_j^n|}{\phi_j^2}\right)}. \end{cases} \tag{7}$$

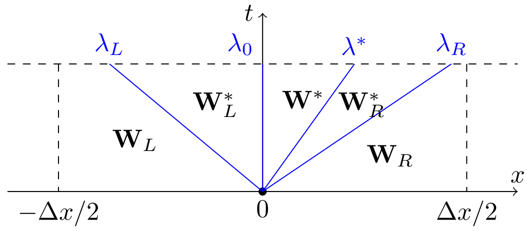

Figure 2. Four-wave approximate solution of Riemann problem.

2.2 A one-dimension Godunov-type scheme

When constructing numerical flux for two-dimension finite volume scheme (5), we have had to project convection equations (4) on the common edge Γ_{jk} of control volumes $C_{j,k}$. Let $\mathbf{W}_{L,R} = R_{\mathbf{n}_{jk}}\mathbf{W}_{j,k}^n$ be the corresponding left- and right-states, we are concerned now to solve the self-similar solution $\mathbf{W}(x/t)$ of one-dimension Riemann problem

$$\begin{cases} \partial_t \mathbf{W} + \partial_x \mathbf{F} = \mathbf{S}_x, \\ \mathbf{W}(x,0) = \begin{cases} \mathbf{W}_L & \text{if} \quad x<0, \\ \mathbf{W}_R & \text{if} \quad x>0, \end{cases} \end{cases} \tag{8}$$

in which $\mathbf{S}_x(\mathbf{W},b) = (0, \frac{g}{2}h^2\partial_x\phi - g\phi h\partial_x b, 0)^T$ is the non-conservative geometrical source term in direction $\mathbf{n}_{jk}$. It is worth noticing that this one-dimension model is equivalent to SW model with breadth variations, see e.g. [11, 12].

As reported in [9], system (8) has three characteristic fields propagating with the following wave speeds

$$\lambda_1 = u - \sqrt{gh}, \quad \lambda_2 = u + \sqrt{gh}, \quad \lambda_3 = u. \tag{9}$$

The two first fields are nonlinear and known to be rarefaction or shock waves while the last field is a contact discontinuity wave. It is shown that the porosity and bathymetry remain constant along all these characteristic wave curves. They may change only across a stationary wave, and along which the following Bernoulli's relation, also called well-balancing property, has to be satisfied

$$\phi hu = \text{const.}, \ \frac{u^2}{2g} + h + b = \text{const.}, \ v = \text{const.}$$

Approximation by simple-solver. Exact solution to the Riemann problem (8) has a complicated structure due to the presence of non-conservative source terms. We consider therefore a simple-solver $\mathbf{W}_{\mathcal{R}}(x/t)$ composed by the given data $\mathbf{W}_L, \mathbf{W}_R$ and three intermediate states $\mathbf{W}_L^*, \mathbf{W}^*, \mathbf{W}_R^*$. They are separated by four discontinuities waves propagating with velocities $\lambda_L \leq \lambda_0 = 0 \leq \lambda_R$ and λ^* as illustrated in Fig. 2. The first order Godunov-type scheme based on this simple-solver can be written as

$$\mathbf{W}_j^{n+1/2} = \mathbf{W}_j^n - \frac{\Delta t}{\Delta x}\left(\mathbf{F}_{j+1/2}^L - \mathbf{F}_{j-1/2}^R\right)$$

where Δx stands for the one-dimension mesh size, and for each cell's interface, the left- and right- numerical fluxes $\mathbf{F}_{j+1/2}^{L,R} = \mathbf{F}^{L,R}(\mathbf{W}_j^n, \mathbf{W}_{j+1}; b_j, b_{j+1})$ are given by

$$\begin{cases} \mathbf{F}^L = \mathbf{F}(\mathbf{W}_L) + \lambda_L(\mathbf{W}_L^* - \mathbf{W}_L) + \lambda_-^*(\mathbf{W}^* - \mathbf{W}_L^*), \\ \mathbf{F}^R = \mathbf{F}(\mathbf{W}_R) - \lambda_R(\mathbf{W}_R - \mathbf{W}_R^*) - \lambda_+^*(\mathbf{W}_R^* - \mathbf{W}^*), \end{cases} \tag{10}$$

with $\lambda_\pm^*$ standing for the positive and negative parts of λ^*. Therefore, the construction of scheme consists in solving intermediate states of the simple-solver. One- and two-dimension fluxes can be linked to each other by relation

$$\mathcal{F}(\mathbf{W}_j^n, \mathbf{W}_k^n; b_j, b_k) = R_{\mathbf{n}_{ij}}^{-1}\mathbf{F}^L(R_{\mathbf{n}_{ij}}\mathbf{W}_j^n, R_{\mathbf{n}_{ij}}\mathbf{W}_k^n; b_j, b_k).$$

Determination of intermediate states. The simple-solver has to be verified an *integral consistency* condition [13] at interface which means that the averaged value of exact solution must be preserved, saying

$$\frac{1}{\Delta x}\int_{-\frac{\Delta x}{2}}^{\frac{\Delta x}{2}} \mathbf{W}_{\mathcal{R}}\left(\frac{x}{\Delta t}\right) \mathrm{d}x = \frac{1}{\Delta x}\int_{-\frac{\Delta x}{2}}^{\frac{\Delta x}{2}} \mathbf{W}\left(\frac{x}{\Delta t}\right) \mathrm{d}x, \tag{11}$$

under a half-CFL condition

$$\Delta t \leq \frac{1}{2}\frac{\Delta x}{\max\{-\lambda_L, \ \lambda_R\}}.$$

It is worth noticing that the factor 1/2 in this CFL condition is rather theoretical; and in practical it is often set to unity. Additional relations on intermediate states can be imposed in order to be consistent with well-balancing property and Riemann invariants of exact solution

$$\phi_L h_L^* u_L^* = \phi_R h_R^* u_R^* := q^*, \tag{12}$$

$$u_L^{*2}/2g + h_L^* + b_L = u_R^{*2}/2g + h_R^* + b_R, \tag{13}$$

$$\begin{cases} v_L^* = v_L, \ v_R^* = v_R, \\ \begin{cases} h^* = h_R^*, \ u^* = u_R^*, \ v^* = v_L^* & \text{if} \quad \lambda^* \geq 0, \\ h^* = h_L^*, \ u^* = u_L^*, \ v^* = v_R^* & \text{otherwise.} \end{cases} \end{cases} \tag{14}$$

Now, let $\mathbf{W}^{HLL}$ denote the usual *HLL-state* of the homogeneous Riemann problem, i.e. without source term,

$$\mathbf{W}^{HLL} = \frac{\lambda_R\mathbf{W}_R - \lambda_L\mathbf{W}_L}{\lambda_R - \lambda_L} - \frac{\mathbf{F}(\mathbf{W}_R) - \mathbf{F}(\mathbf{W}_L)}{\lambda_R - \lambda_L}. \tag{15}$$

Recall that λ_L and λ_R are estimations of slowest and fastest wave speeds. We used in this study a classical estimation based on λ_1 and λ_2 from equation (9), that writes

$$\lambda_L = \min\{0, \ \lambda_1(\mathbf{W}_L), \ \lambda_1(\mathbf{W}_R)\},$$
$$\lambda_R = \max\{0, \ \lambda_2(\mathbf{W}_L), \ \lambda_2(\mathbf{W}_R)\}.$$

Intermediate states of the simple-solver can be seen *a priori* as some perturbations of $\mathbf{W}^{HLL}$ due to the source term $\mathbf{S}_x(\mathbf{W}, b) := (0, S_x, 0)^T$. To see this, we integrate first the conservation law (8) on the rectangular $C =$

$[-\Delta x/2, \Delta x/2] \times [0, \Delta t]$, see again Fig. 2. We use next the consistency (11) and equation (12) to obtain the following relations, after some algebraic manipulations,

$$(\phi h)^{HLL} = \alpha \phi_R h_R^* + (1-\alpha)\phi_L h_L^*, \quad \alpha = \frac{\lambda_R}{\lambda_R - \lambda_L}, \tag{16}$$

$$(\phi hu)^{HLL} = q^* - \frac{\Delta x\, \overline{S_x}}{\lambda_R - \lambda_L}, \quad \overline{S_x} = \frac{1}{|C|}\int_C S_x \,\mathrm{d}x\,\mathrm{d}t. \tag{17}$$

Therefore, by equation (16), which is resulted from mass consistency, $(\phi h)^{HLL}$ is nothing that a convex combination of $\phi_L h_L^*$ and $\phi_R h_R^*$. Equation (17) expresses momentum consistency and allows to compute intermediate discharge q^* from that of HLL-state once given an approximation $\overline{S_x}$ of the source term. We discuss later how such an approximation can be made.

Once q^* is known, we turn now to solve intermediate water depths by employing the well-balancing condition (13). This equation can be rewritten under the form

$$\frac{q^{*2}}{2g}\left(\frac{1}{(\phi_R h_R^*)^2} - \frac{1}{(\phi_L h_L^*)^2}\right) + \frac{\phi_R h_R^*}{\phi_R} - \frac{\phi_L h_L^*}{\phi_L} = b_L - b_R.$$

Combining it with (16), by which $\phi_R h_R^*$ can be seen as function of $\phi_L h_L^*$, the well-balancing condition results thus a nonlinear equation in $\phi_L h_L^*$. Let consider further a natural condition saying that intermediate states have the same regime, i.e. they are both sub-critical or super-critical, this nonlinear equation admits thus an unique and positive solution which can be solved numerically by any iterative method. Solving this (fully) Bernoulli relation allows to provide very accurate result, in particular for the case with large porosity gradient and/or with steep bottom slope.

An alternative approach, which is less accurate but faster and preserves as well steady state at rest, is to replace (13) by a hydrostatic approximation, being $h_L^* + b_L = h_R^* + b_R$. Coupling again with (16) results an explicit expression of intermediate water depths, writing

$$\begin{cases} h_L^* = \dfrac{(\phi h)^{HLL} + \alpha\phi_R(b_R - b_L)}{\alpha\phi_R + (1-\alpha)\phi_L}, \\ h_R^* = \dfrac{(\phi h)^{HLL} - (1-\alpha)\phi_L(b_R - b_L)}{\alpha\phi_R + (1-\alpha)\phi_L}. \end{cases} \tag{18}$$

It remains up to now an estimation for velocity λ^* of the contact discontinuity field. Straightforward calculations from integral consistency condition (11) and Riemann invariants (14) yield

$$\lambda^* = \frac{\phi_L h_L(u_L - \lambda_L) + \phi_R h_R(u_R - \lambda_R) + \lambda_L \phi_L h_L^* + \lambda_R \phi_R h_R^*}{2(\phi h)^*},$$

in which $(\phi h)^*$ standing for the first component of $\mathbf{W}^*$ and thus being $\phi_L h_L^*$ or $\phi_R h_R^*$, depending on the sign of λ^*. Since $(\phi h)^*$ is positive in all case, λ^* is thus well defined once given intermediate water depths h_L^* and h_R^*.

It could be checked that the fluxes $\mathbf{F}^{L,R}$ are nonconservative for second component due to the source term, that is $F_{\phi hu}^L \neq F_{\phi hu}^R$, while they are conservative for first and third components, i.e. $F_{\phi h}^L = F_{\phi h}^R := F_{\phi h}$, $F_{\phi hv}^L = F_{\phi hv}^R := F_{\phi hv}$. In practical, we have not to compute λ^* since straightforward manipulations show that $F_{\phi h}$ and λ^* have the same sign, and furthermore, the flux $F_{\phi hv}$ can be expressed under *upwinding* form

$$F_{\phi hv} = \begin{cases} v_L F_{\phi h} & \text{if} \quad F_{\phi h} \geq 0, \\ v_R F_{\phi h} & \text{otherwise.} \end{cases} \tag{19}$$

Finally, the scheme accounts automatically for the fact that water cannot flow into region of zero porosity. Indeed, considering the case $\phi_R = 0$, equation (16) leads to $-\lambda_L \phi_L h_L^* = (\lambda_R - \lambda_L)(\phi h)^{HLL} = -\lambda_L \phi_L h_L + \phi_L h_L u_L$ and so the flux $F_{\phi h} = 0$ from its definition. Let us remark that this behaviour is due to the adopted structure of simple-solver and, unlike other approaches [4, 5, 9], it does not require any specific approximation of porosity at the interface.

Source term approximation. Deriving an appropriate approximation $\overline{S_x}$ is a key point of the scheme. This consists in defining a *numerical value* of water depth and porosity at the interface, and can be done by investigating well-balancing property. Indeed, considering now the case where $\mathbf{W}_L$ and $\mathbf{W}_R$ are steady states at rest, that is $u_L = u_R = 0$ and $h_L + b_L = h_R + b_R$, these states are preserved by the scheme if $q^* = 0$. Substituting this into momentum consistency equation (17) leads to

$$\begin{aligned} \Delta x\, \overline{S_x} &= \frac{g}{2}\left(\phi_R h_R^2 - \phi_L h_L^2\right) \qquad (20) \\ &= g\left(\frac{h_L h_R}{2}(\phi_R - \phi_L) + \frac{\phi_L h_L + \phi_R h_R}{2}(h_R - h_L)\right) \\ &= g\left(\frac{h_L h_R}{2}(\phi_R - \phi_L) - \frac{\phi_L h_L + \phi_R h_R}{2}(b_R - b_L)\right). \end{aligned}$$

Consequently, we have approximated h^2 by $h_L h_R$ and ϕh by $(\phi_L h_L + \phi_R h_R)/2$ at the interface. As we can see, this approximation is consistent in the sense that $\overline{S_x}$ converges to $S_x(\mathbf{W}, b)$ when $\Delta x \to 0$ and $\mathbf{W}_L, \mathbf{W}_R \to \mathbf{W}$, $b_L, b_R \to b$, in other words when the data and the solution are regular.

To conclude this section, let us summarize the main steps which are useful for practical implementation of proposed method. For convection step (5), we compute first HLL-state $\mathbf{W}^{HLL}$ by (15). Next, we solve intermediate states by providing a source term approximation $\overline{S_x}$, such as (20). This allows to obtain intermediate discharge q^* via (17). After, intermediate water depths $h_{L,R}^*$ are computed by coupling (13) and (16) or by using directly solution (18) which is resulted from hydrostatic approximation. At this stage, we can already calculate the fluxes $\mathbf{F}^{L,R}$ from definition (10) for the two first components and (19) for the last one. We finally take into account the friction and drag force by solving (6) with semi-implicit discretization (7).

3 Numerical experiments

The two first test cases are one-dimension and aim to assess well-balancing property also shock capturing ability of the proposed scheme. Next, a real application of the scheme for macroscopic modelling of open-channel flow with vegetation is found in the third test case, for which numerical results and experimental data are compared.

3.1 Steady sub-critical flow over a bump

The proposed scheme is shown to be well-balanced in the sense that it preserves exactly the steady state at rest, i.e. that with zero discharge. Steady solutions with non-null discharge can also be captured accurately by solving directly Bernoulli relation (13), and not hydrostatic approximation (18), when computing intermediate water depths. To illustrate this, we return to a well-known test case of SW model consisting of steady sub-critical flow over a parabolic bump

$$b(x) = \begin{cases} 0.2 - 0.05(x-10)^2 & \text{if} \quad 8 \le x \le 12, \\ 0 & \text{otherwise.} \end{cases}$$

We impose at upstream an unit discharge $hu = 4.42\text{m}^2/s$ while pre-describe a water depth $h = 2\text{m}$ at downstream. Numerical solutions with $\Delta x = 0.1\text{m}$ are given in Fig. 3. The results allow to highlight that by solving Bernoulli relation the scheme is able to provide very accurate solution, contrary to hydrostatic approximation. Furthermore, one can observe that the present scheme is as efficient as the PorAS scheme [9] for this type of regular solution.

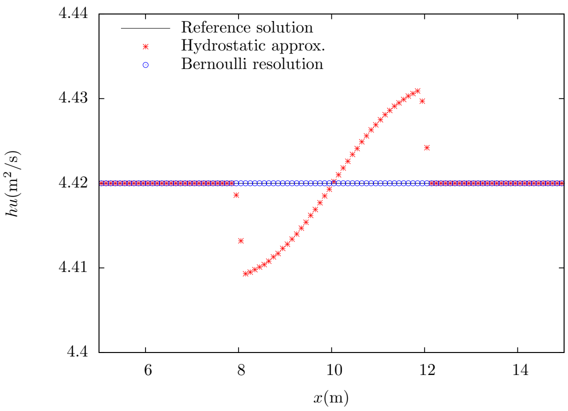

Figure 3. Steady sub-critical flow over a bump. Reference and numerical results for unit discharge with $\Delta x = 0.1\text{m}$.

3.2 Dambreak with large porosity discontinuity

This second test case aims to show an attractive behaviours of the proposed scheme compared to the PorAS one relating on the shock capturing property. We consider a dambreak on flat bottom but with large porosity discontinuity. This test case was proposed in [4] and consists in solving Riemann problem (8) with initial condition

$$(\phi,\ h,\ u) = \begin{cases} (1,\ 10,\ 0) & \text{if} \quad x < 50, \\ (0.1,\ 1,\ 0) & \text{if} \quad x > 50. \end{cases}$$

We notice that discontinuity on porosity at the dam position leads to a complex structure of solution compared to the case of SW model, i.e. with constant porosity. Precisely, from left-state $\mathbf{W}_L$, the solution starts first with a 1-rarefaction wave following by a stationary discontinuity to reach a critical state $\mathbf{W}^*$, that is $u^* = \sqrt{gh^*}$, just after the dam; it continues again with a 1-rarefaction wave and links finally to right-state $\mathbf{W}_R$ by a 2-shock, see Fig 4. Exact solution can be computed by using Riemann invariants, Rankine-Hugoniot relations and well-balancing property.

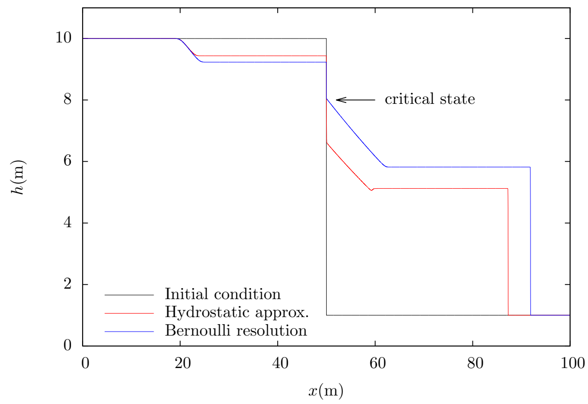

Figure 4. Dambreak with very large porosity discontinuity. The hydrostatic approximation converges to wrong solution.

The proposed scheme with Bernoulli resolution is able to capture correctly the exact solution of Riemann problem while hydrostatic approximation can not, as we can observe on Fig. 4 which is the results at $T = 3\text{s}$ computed with $\Delta x = 10^{-2}\text{m}$. Indeed, this can be understood by the fact that hydrostatic approximation leads to only one intermediate depth because the topography is flat, while solving Bernoulli relation allows to account the discontinuity of porosity. Finally we recall that the construction of PorAS scheme is based on rarefaction waves hypothesis, and, therefore it might present some difficulties when estimating shock waves speed, as noticed in [9] by their authors.

3.3 Transition from meadow to wood

We apply now the SP model solving with the proposed scheme for simulating the flow resistance caused by emergent and rigid vegetation in open-channel flow. We consider here a case of longitudinal transition from meadow to wood in an 18m long and 1m width laboratory flume, and with two types of hydraulic roughness: a bed-roughness figuring a highly submerged dense meadow and emergent macro-roughness figuring a forest. The longitudinal bottom slope was $S_0 = 1.05\text{mm/m}$. Wood-type vegetation was modelled using circular cylinders of diameter $D = 10\text{mm}$, uniformly distributed in staggered rows with density $N = 81$ cylinders/m^2, see Fig. 5 (top). We refer to [14] for more details on experimental setup.

Experimental data reported that the vertical profile of mean velocity, both in meadow and in vegetation regions, remains flat except within a boundary layer. Therefore, explicit simulation with SW model can provide correct result but will leads to very expensive computation cost. Indeed, the circular form of cylinder requires a very high mesh resolution whose the element diameters range typically from 1mm (near the cylinders) to 10mm, see Fig. 5 (bottom).

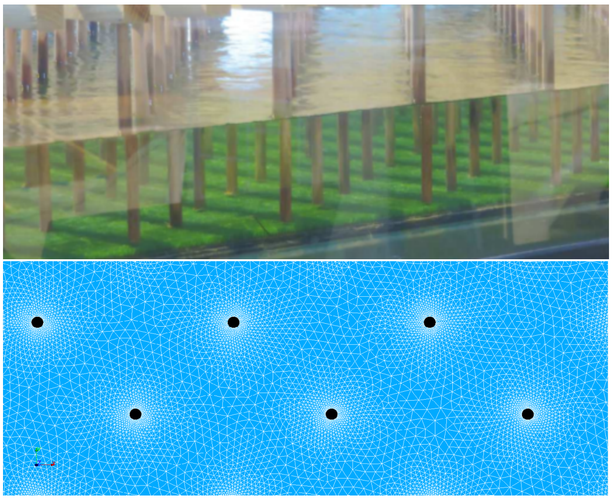

Figure 5. Top: side view of cylinder array (credit: V. Dupuis). Bottom: computational mesh for explicit simulation with TELEMAC-2D (SW model).

This restriction on mesh resolution can of course be relaxed when using SP model. In our study, we used an uniform resolution of 10mm, that is the cylinder's diameter. Next, porosity of the elements close to a cylinder is the ratio of cylinder's area, $\pi D^2/4$, and the total surface occupied by these elements. This simple setting results values of porosity ranging from 0.8 to 0.9. Otherwise, porosity of the elements in water region is set to unity. Numerical simulations were made for the case of uniform discharge $0.015\text{m}^2/\text{s}$, with both SW and SP models. Water depth was imposed at downstream with measured value.

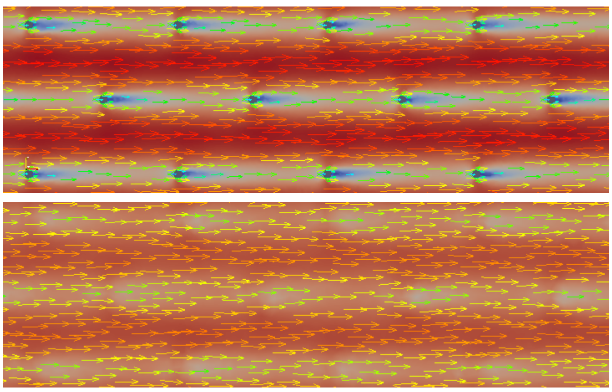

Figure 6. Visualization of velocity field and unit discharge (represented by background color) in vegetation region: SW model (top) and SP model (bottom).

It remains to determine the friction and drag coefficients in order to perform the simulations. One can see *a priori* that the flow is controlled by the bed friction in meadow region while it is dominated by drag force in vegetation region. First, a Strickler roughness coefficient of the meadow was set to $K_s = 60.24\text{m}^{1/3}/\text{s}$ based on the measures from several uniform flows on meadow channel without wood transition, see [15]. This corresponds to a Manning coefficient $n = 1/K_s = 0.0166\text{s/m}^{1/3}$. Next, a simple one-dimension momentum balance equation was used to account the drag force exerted by the cylinders. Drag coefficient was thus evaluated as $C_d = 1.2$, see again [14] for more details. Our first simulation was performed with this *reference* set of values. On Fig. 6 we visualize the velocity field and the unit discharge in vegetation region given by SW and SP models. One can observe that SP model is able to cope macroscopic behaviours: the flow is accelerated between two longitudinal rows of cylinders (called fast vein) while it is decelerated after each cylinder. Slight deviation of flow from the main direction around the cylinders is also observed with SP model.

We turn now to investigate the influence of the transition from bed friction to emergent cylinder drag on longitudinal profile of water depth. Recall that cylinders occupy only on the half last part of the fume, i.e. between $x = 9$m and $x = 18$m. Fig. 7 presents water depths measured along the line $y = 0.5$m with an accuracy of ± 0.5mm. One can observed that the water depth increases upstream of roughness transition, i.e. in meadow region, and becomes nearly constant within vegetation region. This can be understood by the fact that bed friction is negligible compared to drag force in the last part of the flume.

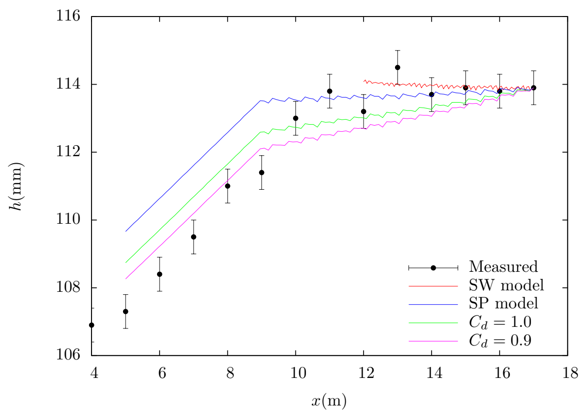

Figure 7. Longitudinal profile of water depth along $y = 0.5$m.

Because of expensive computational cost of SW model, explicit simulation was performed only on a part of vegetation region, from $x = 12$m to $x = 17$m. This simulation allows first to confirm a good agreement between the results of SW and SP models on velocity field, as we have seen before. Next, the water depth predicted by SW model compared to the measured one confirms again that the SW model can be used for detailed modelling of interactions between vegetation and the flow. On the results of SP model, one can see that qualitative behaviours of water depth profile is well captured. Moreover, a good agreement can be found in vegetation region for the result computed with reference value of friction and drag coefficients ($K_s = 60.24$, $C_d = 1.2$, blue curve in Fig. 7). Nevertheless, water depth is overestimated about 2mm in meadow region; this can be improved by imposing a smaller drag coefficient, but in that case, the predictive quality in vegetation part will be reduced. A value $C_d = 1$ seems to be the best compromise for two regions.

4 Conclusion

We have presented in this paper a novel finite volume scheme of Godunov-type for SP model. The solver is based on a four-wave approximation of Riemann problem. This can be seen as an augmented HLLC scheme which is well-balanced, positivity preserving and shock capturing. Details on practical implementation of the scheme were also discussed. Next, a first application to modelling interactions between rigid vegetation with the flow in a laboratory flume was performed. Good agreement was found both with experimental data and the result provided by an explicit simulation with SW model.

Experimental data were provided by the FlowRes projet, supported by the French National Research Agency (ANR) under the grant N^{o}ANR14-CE003-0010. We acknowledge in particular V. Dupuis and S. Proust for their insightful comments.

References

[1] H. Nepf, Water Resources Research **35**, 479 (1999)
[2] H. Nepf, Journal of Hydraulic Research **50**, 262 (2012)
[3] A. Defina, Water Resources Research **36**, 3251 (2000)
[4] V. Guinot, S. Soares-Frazão, Int. J. Numer. Meth. Fluids **50**, 309 (2006)
[5] L. Cea, M.E. Vázquez-Cendón, Int. J. Numer. Meth. Fluids **63**, 903 (2010)
[6] Z.l. Wang, Y.f. Geng, Water Science and Engineering **6**, 91 (2013)
[7] F. Benkhaldoun, I. Elmahi, A. Moumna, M. Seaid, Applicable Analysis **95**, 2181 (2016)
[8] A. Ferrari, R. Vacondio, S. Dazzi, P. Mignosa, Advances in Water Resources **107**, 233 (2017)
[9] P. Finaud-Guyot, C. Delenne, J. Lhomme, V. Guinot, C. Llovel, Int. J. Numer. Meth. Fluids **62**, 1299 (2010)
[10] M.O. Bristeau, B. Coussin, Tech. Rep. 4282, INRIA (2001)
[11] M.J. Castro, A. Pardo, C. Parès, Mathematical Models and Methods in Applied Sciences **17**, 2065 (2007)
[12] N. Goutal, J. Sainte-Marie, Int. J. Numer. Meth. Fluids **67**, 914 (2011)
[13] A. Harten, P.D. Lax, B. van Leer, SIAM Review **25**, 35 (1983)
[14] V. Dupuis, S. Proust, C. Berni, A. Paquier, Environmental Fluid Mechanics **16**, 1173 (2016)
[15] V. Dupuis, Ph.D. thesis, Université de Lyon (2016)